The Astrophysical Journal, 708:1310–1320, 2010 January 10 doi:10.1088/0004-637X/708/2/1310

FERMI OBSERVATIONS OF THE VERY HARD GAMMA-RAY BLAZAR PG 1553+113

A. A. Abdo[1,2], M. Ackermann[3], M. Ajello[3], W. B. Atwood[4], M. Axelsson[5,6], L. Baldini[7], J. Ballet[8], G. Barbiellini[9,10], D. Bastieri[11,12], K. Bechtol[3], R. Bellazzini[7], B. Berenji[3], E. D. Bloom[3], E. Bonamente[13,14], A. W. Borgland[3], J. Bregeon[7], A. Brez[7], M. Brigida[15,16], P. Bruel[17], T. H. Burnett[18], G. A. Caliandro[15,16], R. A. Cameron[3], P. A. Caraveo[19], J. M. Casandjian[8], E. Cavazzuti[20], C. Cecchi[13,14], Ö. Çelik[21,22,23], E. Charles[3], A. Chekhtman[1,24], C. C. Cheung[21], J. Chiang[3], S. Ciprini[13,14], R. Claus[3], J. Cohen-Tanugi[25], J. Conrad[6,26,52], S. Cutini[20], C. D. Dermer[1], A. de Angelis[27], F. de Palma[15,16], E. do Couto e Silva[3], P. S. Drell[3], R. Dubois[3], D. Dumora[28,29], C. Farnier[25], C. Favuzzi[15,16], S. J. Fegan[17], W. B. Focke[3], P. Fortin[17], M. Frailis[27], Y. Fukazawa[30], P. Fusco[15,16], F. Gargano[16], D. Gasparrini[20], N. Gehrels[21,31], S. Germani[13,14], B. Giebels[17], N. Giglietto[15,16], F. Giordano[15,16], T. Glanzman[3], G. Godfrey[3], I. A. Grenier[8], M.-H. Grondin[28,29], J. E. Grove[1], L. Guillemot[28,29], S. Guiriec[32], Y. Hanabata[30], A. K. Harding[21], M. Hayashida[3], E. Hays[21], D. Horan[17], R. E. Hughes[33], G. Jóhannesson[3], A. S. Johnson[3], R. P. Johnson[4], W. N. Johnson[1], T. Kamae[3], H. Katagiri[30], J. Kataoka[34,35], N. Kawai[34,36], M. Kerr[18], J. Knödlseder[37], M. L. Kocian[3], M. Kuss[7], J. Lande[3], L. Latronico[7], M. Lemoine-Goumard[28,29], F. Longo[9,10], F. Loparco[15,16], B. Lott[28,29], M. N. Lovellette[1], P. Lubrano[13,14], G. M. Madejski[3], A. Makeev[1,24], M. N. Mazziotta[16], W. McConville[21,31], J. E. McEnery[21], C. Meurer[6,26], P. F. Michelson[3], W. Mitthumsiri[3], T. Mizuno[30], A. A. Moiseev[22,31], C. Monte[15,16], M. E. Monzani[3], A. Morselli[38], I. V. Moskalenko[3], S. Murgia[3], P. L. Nolan[3], J. P. Norris[39], E. Nuss[25], T. Ohsugi[30], N. Omodei[7], E. Orlando[40], J. F. Ormes[39], M. Ozaki[41], D. Paneque[3], J. H. Panetta[3], D. Parent[28,29], V. Pelassa[25], M. Pepe[13,14], F. Piron[25], T. A. Porter[4], S. Rainò[15,16], R. Rando[11,12], M. Razzano[7], A. Reimer[3,42], O. Reimer[3,42], T. Reposeur[28,29], S. Ritz[4], A. Y. Rodriguez[43], R. W. Romani[3], M. Roth[18], F. Ryde[6,44], H. F.-W. Sadrozinski[4], D. Sanchez[17], A. Sander[33], P. M. Saz Parkinson[4], J. D. Scargle[45], C. Sgrò[7], M. S. Shaw[3], E. J. Siskind[46], D. A. Smith[28,29], P. D. Smith[33], G. Spandre[7], P. Spinelli[15,16], M. S. Strickman[1], D. J. Suson[47], H. Takahashi[30], T. Tanaka[3], J. B. Thayer[3], J. G. Thayer[3], D. J. Thompson[21], L. Tibaldo[8,11,12], D. F. Torres[43,48], G. Tosti[13,14], A. Tramacere[3,49], Y. Uchiyama[3,41], T. L. Usher[3], V. Vasileiou[21,22,23], N. Vilchez[37], V. Vitale[38,50], A. P. Waite[3], P. Wang[3], B. L. Winer[33], K. S. Wood[1], T. Ylinen[6,44,51], and M. Ziegler[4]

[1] Space Science Division, Naval Research Laboratory, Washington, DC 20375, USA
[2] National Research Council Research Associate, National Academy of Sciences, Washington, DC 20001, USA
[3] W. W. Hansen Experimental Physics Laboratory, Kavli Institute for Particle Astrophysics and Cosmology, Department of Physics and SLAC National Accelerator Laboratory, Stanford University, Stanford, CA 94305, USA
[4] Santa Cruz Institute for Particle Physics, Department of Physics and Department of Astronomy and Astrophysics, University of California at Santa Cruz, Santa Cruz, CA 95064, USA
[5] Department of Astronomy, Stockholm University, SE-106 91 Stockholm, Sweden
[6] The Oskar Klein Centre for Cosmoparticle Physics, AlbaNova, SE-106 91 Stockholm, Sweden
[7] Istituto Nazionale di Fisica Nucleare, Sezione di Pisa, I-56127 Pisa, Italy
[8] Laboratoire AIM, CEA-IRFU/CNRS/Université Paris Diderot, Service d'Astrophysique, CEA Saclay, 91191 Gif sur Yvette, France
[9] Istituto Nazionale di Fisica Nucleare, Sezione di Trieste, I-34127 Trieste, Italy
[10] Dipartimento di Fisica, Università di Trieste, I-34127 Trieste, Italy
[11] Istituto Nazionale di Fisica Nucleare, Sezione di Padova, I-35131 Padova, Italy
[12] Dipartimento di Fisica "G. Galilei," Università di Padova, I-35131 Padova, Italy
[13] Istituto Nazionale di Fisica Nucleare, Sezione di Perugia, I-06123 Perugia, Italy
[14] Dipartimento di Fisica, Università degli Studi di Perugia, I-06123 Perugia, Italy
[15] Dipartimento di Fisica, "M. Merlin" dell'Università e del Politecnico di Bari, I-70126 Bari, Italy
[16] Istituto Nazionale di Fisica Nucleare, Sezione di Bari, 70126 Bari, Italy
[17] Laboratoire Leprince-Ringuet, École polytechnique, CNRS/IN2P3, Palaiseau, France; deirdre@llr.in2p3.fr, dsanchez@llr.in2p3.fr, deirdre@in2p3.fr, sanchez@poly.in2p3.fr
[18] Department of Physics, University of Washington, Seattle, WA 98195-1560, USA
[19] INAF-Istituto di Astrofisica Spaziale e Fisica Cosmica, I-20133 Milano, Italy
[20] Agenzia Spaziale Italiana (ASI) Science Data Center, I-00044 Frascati (Roma), Italy
[21] NASA Goddard Space Flight Center, Greenbelt, MD 20771, USA
[22] Center for Research and Exploration in Space Science and Technology (CRESST), NASA Goddard Space Flight Center, Greenbelt, MD 20771, USA
[23] University of Maryland, Baltimore County, Baltimore, MD 21250, USA
[24] George Mason University, Fairfax, VA 22030, USA
[25] Laboratoire de Physique Théorique et Astroparticules, Université Montpellier 2, CNRS/IN2P3, Montpellier, France
[26] Department of Physics, Stockholm University, AlbaNova, SE-106 91 Stockholm, Sweden
[27] Dipartimento di Fisica, Università di Udine and Istituto Nazionale di Fisica Nucleare, Sezione di Trieste, Gruppo Collegato di Udine, I-33100 Udine, Italy
[28] Université de Bordeaux, Centre d'Études Nucléaires Bordeaux Gradignan, UMR 5797, Gradignan 33175, France
[29] CNRS/IN2P3, Centre d'Études Nucléaires Bordeaux Gradignan, UMR 5797, Gradignan 33175, France
[30] Department of Physical Sciences, Hiroshima University, Higashi-Hiroshima, Hiroshima 739-8526, Japan
[31] University of Maryland, College Park, MD 20742, USA
[32] University of Alabama in Huntsville, Huntsville, AL 35899, USA
[33] Department of Physics, Center for Cosmology and Astro-Particle Physics, The Ohio State University, Columbus, OH 43210, USA
[34] Department of Physics, Tokyo Institute of Technology, Meguro City, Tokyo 152-8551, Japan
[35] Waseda University, 1-104 Totsukamachi, Shinjuku-ku, Tokyo 169-8050, Japan
[36] Cosmic Radiation Laboratory, Institute of Physical and Chemical Research (RIKEN), Wako, Saitama 351-0198, Japan
[37] Centre d'Étude Spatiale des Rayonnements, CNRS/UPS, BP 44346, F-30128 Toulouse Cedex 4, France
[38] Istituto Nazionale di Fisica Nucleare, Sezione di Roma "Tor Vergata," I-00133 Roma, Italy

[39] Department of Physics and Astronomy, University of Denver, Denver, CO 80208, USA
[40] Max-Planck Institut für extraterrestrische Physik, 85748 Garching, Germany
[41] Institute of Space and Astronautical Science, JAXA, 3-1-1 Yoshinodai, Sagamihara, Kanagawa 229-8510, Japan
[42] Institut für Astro- und Teilchenphysik and Institut für Theoretische Physik, Leopold-Franzens-Universität Innsbruck, A-6020 Innsbruck, Austria
[43] Institut de Ciencies de l'Espai (IEEC-CSIC), Campus UAB, 08193 Barcelona, Spain
[44] Department of Physics, Royal Institute of Technology (KTH), AlbaNova, SE-106 91 Stockholm, Sweden
[45] Space Sciences Division, NASA Ames Research Center, Moffett Field, CA 94035-1000, USA
[46] NYCB Real-Time Computing Inc., Lattingtown, NY 11560-1025, USA
[47] Department of Chemistry and Physics, Purdue University Calumet, Hammond, IN 46323-2094, USA
[48] Institució Catalana de Recerca i Estudis Avançats (ICREA), Barcelona, Spain
[49] Consorzio Interuniversitario per la Fisica Spaziale (CIFS), I-10133 Torino, Italy
[50] Dipartimento di Fisica, Università di Roma "Tor Vergata," I-00133 Roma, Italy
[51] School of Pure and Applied Natural Sciences, University of Kalmar, SE-391 82 Kalmar, Sweden
Received 2009 August 14; accepted 2009 November 24; published 2009 December 21

ABSTRACT

We report the observations of PG 1553+113 during the first ∼200 days of *Fermi Gamma-ray Space Telescope* science operations, from 2008 August 4 to 2009 February 22 (MJD 54682.7–54884.2). This is the first detailed study of PG 1553+113 in the GeV gamma-ray regime and it allows us to fill a gap of three decades in energy in its spectral energy distribution (SED). We find PG 1553+113 to be a steady source with a hard spectrum that is best fit by a simple power law in the *Fermi* energy band. We combine the *Fermi* data with archival radio, optical, X-ray, and very high energy (VHE) gamma-ray data to model its broadband SED and find that a simple, one-zone synchrotron self-Compton model provides a reasonable fit. PG 1553+113 has the softest VHE spectrum of all sources detected in that regime and, out of those with significant detections across the *Fermi* energy bandpass so far, the hardest spectrum in that energy regime. Thus, it has the largest spectral break of any gamma-ray source studied to date, which could be due to the absorption of the intrinsic gamma-ray spectrum by the extragalactic background light (EBL). Assuming this to be the case, we selected a model with a low level of EBL and used it to absorb the power-law spectrum from PG 1553+113 measured with *Fermi* (200 MeV–157 GeV) to find the redshift, which gave the best fit to the measured VHE data (90 GeV–1.1 TeV) for this parameterization of the EBL. We show that this redshift can be considered an upper limit on the distance to PG 1553+113.

Key words: BL Lacertae objects: individual (PG 1553+113) – gamma rays: observations

Online-only material: color figure

1. INTRODUCTION

PG 1553+113 is a high-frequency peaked BL Lacertae object (HBL; Falomo et al. 1994; Beckmann et al. 2002) whose redshift remains unknown despite continued efforts to determine it. Like all BL Lacs, we find its spectral energy distribution (SED) to have a double-peaked shape (in $\nu F\nu$ representation) that can thus be parameterized with four characteristic slopes. It has been detected from radio through hard X-rays and also in the very high energy (VHE; $E \gtrsim 100$ GeV) regime up to energies above 1 TeV (Aharonian et al. 2006b; Albert et al. 2007). With these data, three of the four components of its SED were sampled, namely, the rising and falling edges of the low-energy peak ($\sim 10^{-6}$ eV–30 keV) and the falling edge of the high-energy peak (∼90 GeV–1 TeV). We report here the first detailed analysis of the rising high-energy portion and, crucially, the high-energy peak, of the PG 1553+113 SED. These data, from observations made by the *Fermi Gamma-ray Space Telescope* Large Area Telescope (*Fermi* LAT; Atwood et al. 2009) during its first ∼200 days of operation, are combined with data from other wavebands to construct and model the broadband SED of PG 1553+113 in Section 4.1.

Discovered and classified as a BL Lacertae object (BL Lac) by Green et al. (1986), PG 1553+113 is located at an R.A. of $\alpha_{J2000} = 15^{\rm h}55^{\rm m}43\overset{\rm s}{.}04$ and a declination of $\delta_{J2000} = +11^{\rm d}11^{\rm m}24\overset{\rm s}{.}4$ in the constellation of Serpens Caput. The logarithmic ratio of its 5 GHz radio flux, $F_{5\,\rm GHz}$, to its 2 keV X-ray flux, $F_{2\,\rm keV}$, has been found to range from $\log(F_{2\,\rm keV}/F_{5\,\rm GHz}) = -4.99$ to -3.88 (Osterman et al. 2006; Rector et al. 2003). The high value of this ratio places PG 1553+113, at times, among the most extreme of the HBLs; a BL Lac is classified as extreme when it has $\log(F_{2\,\rm keV}/F_{5\,\rm GHz}) \geqslant -4.5$ (Rector et al. 2003). A number of the TeV blazars have, at one time or another, exhibited fluxes that place them in this extreme category (e.g., 1ES 0229+200, H 1426+428, 1ES 1959+650; Rector et al. 2003).

In the radio band, PG 1553+113 has been detected at different mean flux levels. Its 4.8 GHz flux, for example, has ranged from 180 to 675 mJy (Bennett et al. 1986; Gregory & Condon 1991; Becker et al. 1991; Perlman et al. 2005; Osterman et al. 2006). Its flux between 4.8 and 14.5 GHz was found to be variable on month timescales during the observations of Perlman et al. (2005) and Osterman et al. (2006). Very Long Baseline Array (VLBA) observations have resolved a jet extending at least 20 pc to the northeast of PG 1553+113 (Rector et al. 2003). No evidence for superluminal motion has been reported in the literature to date; multi-epoch VLBA monitoring has commenced recently.[53]

PG 1553+113 is a bright optical source with *V*-band magnitude of $V_o \sim 14$ (Falomo & Treves 1990; Osterman et al. 2006). Observations taken between 1986 and 1991 with the ESO telescopes found its spectral index, α_o, to remain almost constant ($\alpha_o \sim -1$) and its magnitude to vary by $\Delta V_o = 1.4$ (Falomo et al. 1994). Low levels of optical variability were seen by

[52] Royal Swedish Academy of Sciences Research Fellow, funded by a grant from the K. A. Wallenberg Foundation.

[53] http://web.whittier.edu/gpiner/research/index.htm

Table 1
The Flux and Spectral Parameters from X-ray Observations (2–10 keV, Unless Otherwise Noted) of PG 1553+113

Observatory	Observation Date(s)	Flux (2–10 keV) ($\times 10^{-11}$ erg cm^{-2} s^{-1})	Spectral Parameters		
		[Ref.]	a	b	[Ref.]
ASCA	1995 Aug 16	2.9 [Don01]	2.47	...	[Don01]
BeppoSAX	1998 Feb 05	1.4 [Don05]	2.17	0.63	[Mas08]
XMM-Newton	2001 Sep 06	3.5 [Per05]	2.09	...	[Mas08]
RXTE	2003 Apr 22 to 2003 May 12[a]	0.7 [Ost06]	2.37	...	[Ost06]
	2003 Apr 22 to 2003 May 28[b]	0.5 [Ost06]	2.60	...	[Ost06]
	2003 Apr 26[c]	0.3 [Ost06]	3.19	...	[Ost06]
	2003 May 11[d]	1.2 [Ost06]	2.26	...	[Ost06]
Swift-XRT	2005 Apr 20	2.1 [Tra07]	2.21	0.36	[Mas08]
	2005 Oct 06	6.9 [Tra07]	2.14	0.24	[Mas08]
	2005 Oct 08	6.7 [Tra07]	2.11	0.23	[Mas08]
Suzaku	2006 Jul 24 to 2006 Jul 25	3.5 [Rei08]	2.19	0.26[e]	[Rei08]

Notes. The spectral parameters for a log–parabola fit are shown with the differential X-ray flux, $F_X(\mathrm{E}) \propto \mathrm{E}^{-a-b(\log(E))}$ (cm^{-2} s^{-1} keV^{-1}). In cases where no value is given for b, the best-fit power-law spectrum is shown with $F_X(E) \propto E^{-a}$ (cm^{-2} s^{-1} keV^{-1}). The abbreviated references correspond to the following: [Don01]: Donato et al. 2001; [Don05]: Donato et al. 2005; [Per05]: Perlman et al. 2005; [Ost06]: Osterman et al. 2006; [Tra07]: Tramacere et al. 2007; [Rei08]: Reimer et al. 2008; [Mas08]: Massaro et al. 2008.

[a] The mean flux and spectral index during the whole campaign.

[b] The mean flux and spectral index prior to the flare.

[c] The minimum flux recorded during the campaign and the spectral index at that time.

[d] The maximum flux recorded during the campaign and the spectral index at that time.

[e] The *Suzaku* spectrum was measured between 0.3 and 30 keV.

Osterman et al. (2006) during their 2003 observing campaign. Limits on the magnitude of its host galaxy will be discussed later.

PG 1553+113 is also a bright X-ray source that has been observed by most X-ray missions (*Einstein*, *ROSAT*, *ASCA*, *BeppoSAX*, *RXTE*, *XMM-Newton*, *Swift*, and *Suzaku*). Although it has been detected at a number of different flux levels by these observatories, no evidence for strong or fast (sub-hour) flux variability has been observed at X-ray energies (Reimer et al. 2008). The *Suzaku* observations performed in 2006 July (Reimer et al. 2008) provide the highest energy X-ray measurement so far obtained for PG 1553+113 at ∼30 keV with a 10–30 keV flux of 1.35×10^{-11} erg cm^{-2} s^{-1}. No evidence for spectral hardening up to these energies was found in these data, indicating that all of the X-ray emission detected was due to synchrotron emission. The 2–10 keV fluxes measured by different X-ray missions are shown in Table 1, the highest being 6.9×10^{-11} erg cm^{-2} s^{-1} in 2006 October (*Swift-XRT*; Tramacere et al. 2007). The X-ray flux was found to double over a period of 10 days during the three-week *RXTE* observing campaign of Osterman et al. (2006). Despite the variations of a factor of approximately 20 in the 2–10 keV X-ray flux, the measured spectral properties of PG 1553+113 at these energies, also listed in Table 1, have not changed significantly over the course of the X-ray observations. It exhibits spectral curvature that can be well described with either a broken power law or a log–parabolic shape. In the *Suzaku* data, this curvature extends into the hard X-ray band ($\leqslant 30$ keV) and steepening of the spectrum above ∼10 keV, beyond that predicted by either the broken power-law or log–parabolic model is observed (Reimer et al. 2008).

In the high energy (HE; $E \sim 100$ MeV–100 GeV) gamma-ray regime, PG 1553+113 was not detected by EGRET. An upper limit of $F_{\mathrm{EGRET}} < 9.97 \times 10^{-8}$ cm^{-2} s^{-1} above 100 MeV was derived based on the summed exposure of cycles 1, 2, 3, and 4 (Hartman et al. 1999). At higher energies, in the VHE regime, PG 1553+113 is a confirmed gamma-ray emitter. First detected by H.E.S.S. (Aharonian et al. 2006b) and subsequently confirmed by MAGIC (Albert et al. 2007), PG 1553+113 has a flux that is approximately 3% that of the Crab Nebula at these energies. The combined 2005–2006 H.E.S.S. data follow a power law with photon index of $\Gamma_{\mathrm{VHE}} = 4.46 \pm 0.34$ between ∼225 GeV and 1.3 TeV (Aharonian et al. 2008). The MAGIC 2005–2006 spectra are consistent with this having a power-law photon index of $\Gamma_{\mathrm{VHE}} = 4.21 \pm 0.25$ between ∼90 and 500 GeV (Albert et al. 2007). No evidence for variability of the spectral index, to within the measurement uncertainties, is seen in the VHE measurements. The H.E.S.S. and MAGIC integral flux levels are consistent from 2005 April to August and from 2006 April to July with a mean flux of I_{VHE} ($E > 200$ GeV) $= 2.0 \pm 0.8 \times 10^{-11}$ cm^{-2} s^{-1}. Although the spectrum remained unchanged, the flux detected by MAGIC between 2006 January and April was lower than the preceding and proceeding measurements at I_{VHE} ($E > 200$ GeV) $= 0.6 \pm 0.2 \times 10^{-11}$ cm^{-2} s^{-1}. When the systematic uncertainties on the fluxes are taken into account, this flux is marginally inconsistent with the VHE fluxes detected during the H.E.S.S. and other MAGIC observations suggesting that the PG 1553+113 flux varied by up to a factor of 3 on monthly timescales in 2006. PG 1553+113 has the steepest spectrum of all of the sources detected in the VHE regime, which makes it a promising target for the *Fermi* LAT because extrapolating down to the *Fermi* energy range would make this an extremely bright source unless a dramatic spectral break occurs at energies below ∼100 GeV. EGRET's non-detection could be interpreted in this context or as the result of PG 1553+113 being in a lower emission state at that time than during the VHE observations. PG 1553+113 is in the *Fermi* LAT bright active galactic nucleus (AGN) source list (LBAS; Abdo et al. 2009a), the high-confidence AGN associations from the first three months of *Fermi* data. Listed as 0FGL J1555.8+1110 with a flux of I_{LBAS} ($E > 100$ MeV) $= 8.0 \pm 1.0 \times 10^{-8}$ cm^{-2} s^{-1} and a photon index of $\Gamma_{\mathrm{LBAS}} = 1.70 \pm 0.06$, it has one of the hardest spectra of the 106 AGNs that comprise this list. Indeed,

if only the AGNs with a significant detection across the entire *Fermi* bandpass are considered, its spectrum is the hardest of those in the LBAS. This combination of a very soft VHE spectrum and a very hard HE spectrum means that PG 1553+113 has a significant spectral break in the gamma-ray regime.

Despite significant efforts to determine the redshift of PG 1553+113, it remains unknown. Its measurement is of great interest both for a better understanding of its SED, in particular, since it is an extreme BL Lac and therefore has a very hard synchrotron emission spectrum, and also for studying extragalactic background light (EBL) effects; some redshift estimates make it the most distant VHE source detected to date at $z < 0.78$ (Sbarufatti et al. 2005), which, if shown to be the case, could imply an EBL density close to the minimum allowed by galaxy counts. The results of redshift studies undertaken to date are summarized in Section 3 and the archival gamma-ray data together with the *Fermi* data from PG 1553+113 are used to place constraints on its redshift.

2. *FERMI* OBSERVATIONS OF PG 1553+113

The characteristics and performance of the LAT Instrument on the *Fermi Gamma-ray Space Telescope* are described in detail by Atwood et al. (2009). Presented here is the analysis of the *Fermi* LAT data from a region of 10° radius centered on PG 1553+113 from 2008 August 4 to 2009 February 22 (MJD 54682.7-54884.2).[54] These data were analyzed using the standard *Fermi* analysis software.[55] Events with zenith angles <105° were selected from the so-called "diffuse class," those events having the highest probability of being a photon. Only events with energies greater than 200 MeV were used in this analysis. The extragalactic diffuse gamma-ray emission together with the residual instrumental background was modeled as a simple power law while the galactic diffuse was modeled with *GALPROP*[56] (Strong et al. 2004b; Strong et al. 2004a).

There are two other *Fermi* sources within 10° of PG 1553+113. These sources, lying at angular separations of 1.°8 and 5.°5 from PG 1553+113 were modeled in our analysis so that they could be subtracted out along with the backgrounds described above. The nearest source to PG 1553+113, 0FGL J1553.4+1255, is located at R.A. $\alpha_{J2000} = 15^{\rm h}53^{\rm m}28\overset{\rm s}{.}2$ and declination $\delta_{J2000} = +12^{\rm d}55^{\rm m}20\overset{''}{.}3$ and is thus spatially coincident with the quasar QSO B1551+1305 ($z = 1.29$). It is detected up to approximately 10 GeV with an integral flux ($E > 200$ MeV) of $5.67 \pm 0.38 \times 10^{-8}$ cm^{-2} s^{-1} and photon index of 2.26 ± 0.05. There is evidence for variability in its photon index and flux but neither are correlated with the signal detected from PG 1553+113. The LAT has a point-spread function (PSF), θ_{68}, that decreases with increasing energy.[57] For energies above 360 MeV, the PSF of the LAT is smaller than 1.°8, the angular separation between PG 1553+113 and 0FGL J1553.4+1255. Therefore, for almost all of the energy range over which the PG 1553+113 data are analyzed here ($E = 200$ MeV–400 GeV), the PSF of the LAT is such that the PG 1553+113 data are not significantly contaminated by the signal from 0FGL J1553.4+1255. To ensure that this was the case, we performed an analysis of the PG 1553+113 data with energy $E > 400$ MeV. The results obtained from this analysis are entirely consistent with those obtained when the full energy range ($E > 200$ MeV) is considered.

The other source within 10° of PG 1553+113 is not in the LBAS. It is located at an R.A. of $\alpha_{J2000} = 16^{\rm h}07^{\rm m}40\overset{\rm s}{.}5$ and a declination of $\delta_{J2000} = +15^{\rm d}50^{\rm m}36\overset{''}{.}2$ and was detected up to approximately 10 GeV with an integral flux ($E > 200$ MeV) of $2.06 \pm 0.28 \times 10^{-8}$ cm^{-2} s^{-1} and photon index of 2.31 ± 0.11. Its angular separation of 5.°5 from PG 1553+113 is well in excess of the width of the *Fermi* PSF over the full energy range.

In the *Fermi* data analyzed here, PG 1553+113 was detected with a statistical significance of approximately 49σ (`gtlike` calculated a test significance[58] of 2407) and an integral flux I ($E > 200$ MeV) of $5.00 \pm 0.31 \times 10^{-8}$ cm^{-2} s^{-1}. The most energetic photon in the *Fermi* data is at 157 GeV (at an angular separation of 0.°04 from the source location, i.e., well within θ_{68} for that energy). The *Fermi* data are well described by a power law such that the differential photon flux, $F(E)$, is given by:

$$F(E) = \frac{dN}{dE} = F_0 \left(\frac{E}{E_0}\right)^{-\Gamma}, \quad (1)$$

where F_0 is the differential flux at energy, E_0, and Γ is the photon index. For each energy, E, the uncertainty contours, called the butterfly, are defined such that the differential flux satisfies:

$$\frac{\Delta F^2}{F^2} = \left(\frac{\Delta F_0}{F_0}\right)^2 + \ln^2\left(\frac{E}{E_0}\right)\Delta\Gamma^2 - \frac{2}{F_0}\,\mathrm{cov}(F_0, \Gamma)\ln\left(\frac{E}{E_0}\right), \quad (2)$$

where $\mathrm{cov}(F_0, \Gamma)$ is the covariance term, returned by the `MINUIT` minimization and error analysis function called by the *Fermi* likelihood analysis tool, `gtlike`, and ΔF, ΔF_0 and $\Delta\Gamma$ are the statistical uncertainties on the F, F_0, and Γ, respectively, at energy, E. Equation (2) reaches a minimum at the decorrelation energy, $E_{\rm dec}$, where:

$$E_{\rm dec} = E_0 \exp\left(\frac{\mathrm{cov}(F_0, \Gamma)}{F_0\Delta\Gamma^2}\right), \; F_{\rm dec} \equiv F(E_{\rm dec}). \quad (3)$$

For the PG 1553+113 data analyzed here, we find a differential flux of $F_{\rm dec} = 2.60 \pm 0.18 \times 10^{-9}$ cm^{-2} s^{-1} GeV^{-1} with $E_{\rm dec} = 2.4$ GeV and a photon index of $\Gamma = 1.68 \pm 0.03$. The differential energy spectrum with the butterfly is shown in Figure 1. Also plotted are the fluxes calculated when the data were analyzed in eight independent energy bins fixing the photon index in each bin to that derived from the entire data set, since the preferred fit to this was a power law. These fluxes are listed in Table 2. To estimate the systematic uncertainties on the PG 1553+113 flux and photon index, the PG 1553+113 data were reanalyzed using two new sets of instrument response functions (IRFs; Atwood et al. 2009) that were created by propagating both extremes of the uncertainties on IRF `P6_V3_DIFFUSE`. From this analysis, we estimate the systematic uncertainties to be at the level of 2% on the photon index ($\Gamma = 1.68 \pm 0.03_{\rm stat}\,^{+0.02}_{-0.04{\rm syst}}$) and 3% on the differential flux ($F_{\rm dec} = 2.60 \pm 0.18_{\rm stat}\,^{+0.09}_{-0.08{\rm syst}} \times 10^{-9}$ cm^{-2} s^{-1} GeV^{-1}).

[54] Mission Elapsed Time 239,557,414 to 256,966,310 s.

[55] `ScienceTools v9r10` with IRF `P6_V3_DIFFUSE` (Atwood et al. 2009).

[56] The background file `mapcube_54_59Xvarh7S.fits` was used.

[57] The accurate parameterization of the LAT PSF to be used for science analysis is described by the instrument IRF. The following simplified, acceptance-averaged approximation for the 68% containment angle might be useful as an illustration of the PSF energy dependence:
$\theta_{68} \simeq \sqrt{(0.°8 \times E_{\rm GeV}^{-0.8})^2 + (0.°07)^2}$.

[58] The test significance is defined as $-2\ln(\Lambda)$, where Λ is the likelihood ratio for the null hypothesis and the assumed source model; see Abdo et al. (2009b) for a full description.

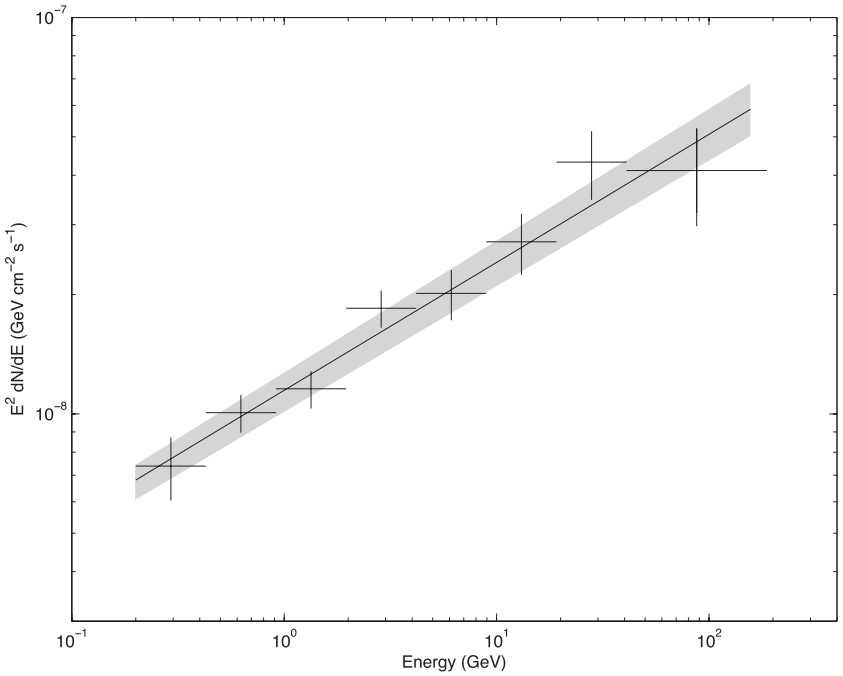

Figure 1. Differential spectrum from PG 1553+113 as measured by *Fermi*. The solid line shows the fit of a power law to the overall spectrum derived from all of the data with energy $E > 200$ MeV. The data points (crosses) indicate the flux measured in each of the eight energy bins indicated by the extent of their horizontal lines, when the data in these energy ranges were analyzed with the photon index fixed at the value derived from the entire data set. The gray shaded area shows the extent of the *Fermi* 68% confidence band.

Table 2
The Differential Flux Measured by the *Fermi* LAT in Each Energy Bin

Energy Range (GeV)	Flux (cm^{-2} s^{-1} GeV^{-1})
0.20–0.43	$8.63 \pm 1.56 \times 10^{-8}$
0.43–0.92	$2.57 \pm 0.28 \times 10^{-8}$
0.92–1.96	$6.46 \pm 0.70 \times 10^{-9}$
1.96–4.18	$2.26 \pm 0.24 \times 10^{-9}$
4.18–8.94	$5.38 \pm 0.78 \times 10^{-10}$
8.94–19.13	$1.59 \pm 0.28 \times 10^{-10}$
19.13–40.90	$5.52 \pm 1.08 \times 10^{-11}$
40.90–187.05	$5.37\,^{+1.49}_{-1.16}{}^{a} \times 10^{-12}$

Note. [a] The uncertainty in the highest energy bin is found to be asymmetric.

The PG 1553+113 200-day light curves for the integral flux, $I_{2\,\mathrm{Day}}$ ($E > 200$ MeV), and the photon index, $\Gamma_{2\,\mathrm{Day}}$, with 2-day binning are shown in Figure 2. This timescale was chosen so that a detection with a statistical significance of at least 3σ was obtained in most bins. These are the longest continuous light curves ever derived for this source. The χ^2 probability of the data being fit by a constant are 0.54 and 0.99, respectively, for the integral fluxes and the photon indices. The normalized excess variance (Vaughan et al. 2003) is $\sigma^2_{NXS} = -2.7 \times 10^{-2}$ for the flux light curve and $\sigma^2_{NXS} = -1.6 \times 10^{-2}$ for the photon index light curve.[59] Both of these calculations suggest that, to within measurement uncertainties, the flux and photon index from PG 1553+113 were constant during these observations. Assuming this to be the case, an upper limit on the intrinsic variability that could be present in the flux light curve was derived as follows. An ensemble of light curves, each with a different level of intrinsic Gaussian noise added, was simulated. For each level of intrinsic variability, v_i, 1000 light curves, each the same length, L, as the measured light curve were generated. Each flux point in these light curves, $(I_{\mathrm{sim}})_{ij} \pm (\Delta I_{2\,\mathrm{Day}})_j$ ($1 \leqslant j \leqslant L$), was drawn from a Gaussian distribution centered on the mean of the measured light curve with width of $\sqrt{\left(\Delta I^2_{2\,\mathrm{Day}}\right)_j + v_i^2}$, where $(\Delta I_{2\,\mathrm{Day}})_j$ is the measurement uncertainty for the jth measured flux. For each of these simulated light curves, the excess variance was calculated, providing a distribution of 1000 simulated excess variance measurements for each level of added intrinsic variability. For each of these distributions, the value above which 95% of the excess variances lay was found. With these data, upper limits were calculated by constructing a Neyman confidence belt. It was found that, at the 95% confidence level, the upper limit on the normalized intrinsic variance from the PG 1553+113 flux is $v < 7.8 \times 10^{-2}$. The same procedure was applied to the photon index light curve and an upper limit of $v < 1.4 \times 10^{-2}$ at the 95% confidence level was derived for the normalized intrinsic variance on the PG 1553+113 photon index.

3. USING THE GAMMA-RAY DATA TO CONSTRAIN THE REDSHIFT OF PG 1553+113

For many years, PG 1553+113 was thought to lie at a redshift of $z = 0.36$ (Miller & Green 1983). This redshift estimate was based on a spurious emission line in its spectrum, misidentified as Lyman-α (Falomo & Treves 1990). Subsequent observations have failed to reveal any spectral features (Falomo & Treves 1990; Falomo et al. 1994; Carangelo et al. 2003). Since its detection in the VHE band, a number of dedicated observing campaigns and reanalyses of *Hubble Space Telescope* (*HST*) images have been undertaken to determine its redshift but, despite

[59] It is possible to arrive at a negative value for σ^2_{NXS} when there is low intrinsic variance and/or the measurement uncertainties are overestimated.

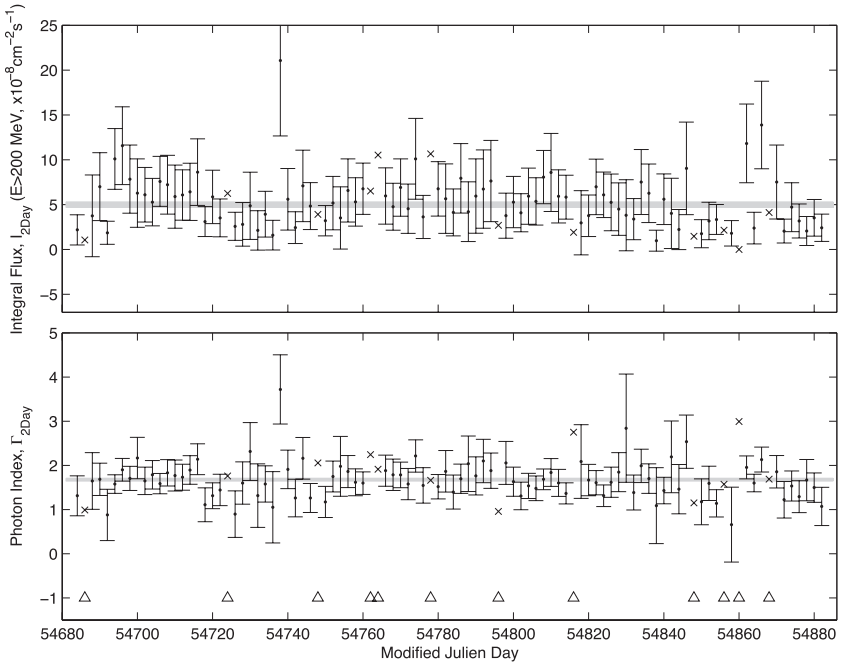

Figure 2. Light curve for PG 1553+113 measured by *Fermi* between MJD 54683 and 54883 (2008-08-05–2009-02-21). The data are binned in two-day bins. The top panel shows the integral flux, $I_{2\,\mathrm{Day}}$ ($E > 200$ MeV), for each two-day bin. The bottom panel shows the power-law photon index, $\Gamma_{2\,\mathrm{Day}}$, for each two-day bin. The integral flux and photon index, with their uncertainties, calculated by `gtlike` for the entire data set are shown by the shaded horizontal bands. For twelve of the timebins, indicated by the triangles in the lower panel, the analysis failed to converge with reasonable error bars and therefore, these data were excluded from the variability analysis and the points are shown as "×" symbols.

these efforts, the redshift of PG 1553+113 remains unknown, (Sbarufatti et al. 2005, 2006; Treves et al. 2007; Aharonian et al. 2008). Constraints, some of them contradictory, have been placed on its redshift using a variety of techniques. These fall into two categories—spectral and imaging observations in optical to ultraviolet wavebands and VHE gamma-ray spectral observations.

The host galaxy of PG 1553+113 was neither resolved by Hutchings & Neff (1992) using the High-Resolution camera on the Canada France Hawaii Telescope nor by Scarpa et al. (2000) who observed it as part of a survey of 110 BL Lacs using *HST*. The host galaxies of 69 out of these were resolved by *HST*, including almost all objects with $z < 0.5$. Sbarufatti et al. (2005) analyzed these *HST* data and showed that the host galaxy luminosity is encompassed in a relatively narrow range for the BL Lacs resolved with *HST*, thus concluding that BL Lac host galaxies typically have absolute magnitude of $M_R = -22.8$. They used this assumption to derive lower limits on the redshifts for those objects lying at unknown distances for which no host galaxy could be resolved, thus arriving at a lower limit of $z > 0.78$ for PG 1553+113, the brightest such object in the survey. Using a similar strategy, Carangelo et al. (2003) set a lower limit of $z > 0.3$ on the redshift of PG 1553+113 using preliminary results from observations with the ESO 3.6 m telescope. Treves et al. (2007) reanalyzed the *HST* image of PG 1553+113 and, again making the assumption that its host galaxy is typical of BL Lacs, placed a lower limit of $z \geqslant 0.25$ on the redshift. In comparing their results with those from VHE observations, they concluded that its redshift is in the range $z = 0.3 - 0.4$. Sbarufatti et al. (2006) used the ESO VLT to measure the optical spectra of a number of BL Lacs including PG 1553+113. Combining the fact that no spectral features were resolved with their knowledge of the sensitivity of the VLT to such features, they were able to derive a lower limit of $z > 0.09$ on the redshift PG 1553+113, under the assumption that its host galaxy is typical.

All of the results above, however, rely on the result of Sbarufatti et al. (2005), which states that BL Lac host galaxies have a very small dispersion in their absolute magnitudes. The results of a study by O'Dowd & Urry (2005) casts doubt on the validity of this assumption for objects with $z > 0.5$ because they find evidence for strong evolution in the host galaxies of BL Lacs in the redshift range of $z = 0.5$–2.5.

Gamma-ray data can be used indirectly to estimate redshifts provided that a few necessary assumptions are valid. The VHE spectra of extragalactic sources whose redshifts are known can be used to probe the density of the EBL because the high-energy gamma rays produce e^+e^- pairs with the EBL photons thus introducing a redshift-dependent absorption feature on the spectra observed in the VHE regime (Costamante et al. 2004; Dwek & Krennrich 2005; Stecker et al. 2007; Krennrich et al. 2008). Conversely, in cases such as that of PG 1553+113, a firmly established VHE source (Aharonian et al. 2006b, 2008; Albert et al. 2007, 2009) lying at an unknown distance, the measured spectrum can be used in combination with assumptions about the density of the EBL and the intrinsic VHE spectrum to put limits on its redshift. By assuming a minimal level of EBL (Primack et al. 2001) and that the intrinsic spectrum of PG 1553+113 is unlikely to have a photon index harder than $\Gamma_{\mathrm{int}} = 1.5$, the limit from shock acceleration models (Aharonian et al. 2006a), Aharonian et al. (2006b) derived an upper limit of $z < 0.74$ on its redshift. We note that none of the *Fermi* LBAS sources that have significant detections across the entire *Fermi* bandpass have photon indices harder than 1.5, providing additional support for the validity of this assumption. When these data were reanalyzed and combined with subsequent H.E.S.S. data, a refined upper limit of $z < 0.69$ was calculated (Aharonian et al. 2008). A similar procedure was adopted by Albert et al.

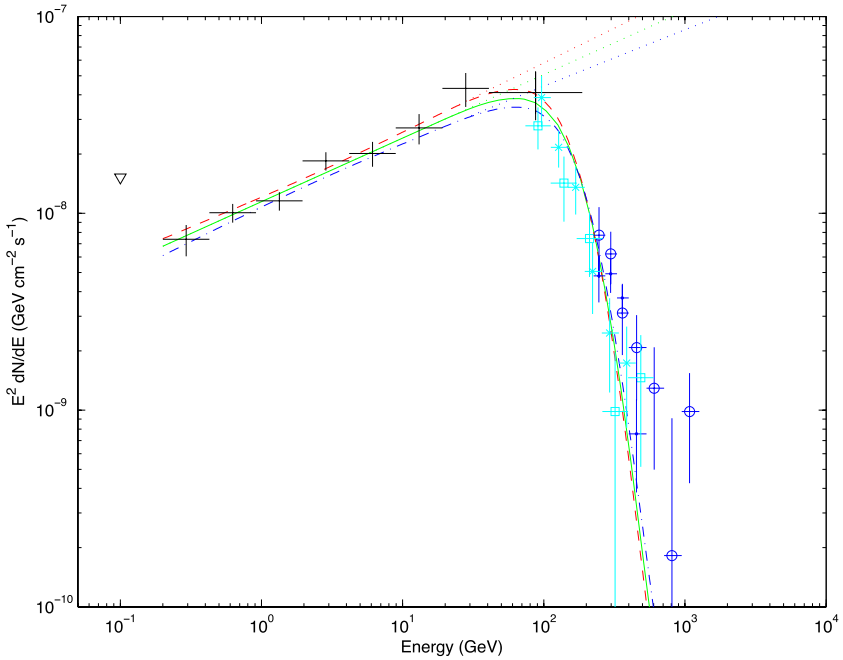

Figure 3. SED for the gamma-ray data. The individual data sets are described in the text. The *Fermi* data points are shown as black crosses. The EGRET upper limit for emission above 100 MeV is shown as a black triangle. The H.E.S.S. data combined from 2005 May and August are shown as blue dots and those combined from 2006 April and July as blue open circles. The MAGIC data combined from 2005 April and May and from 2006 January to April are shown as cyan x's while those from 2006 July are shown as cyan open squares. The green solid line shows the power-law fit to the *Fermi* data, extended to higher energies with the level of EBL that best fitted the VHE data, which corresponds to the EBL integrated to a redshift of $z = 0.75$. The green dotted line shows the extension of the *Fermi* power law to higher energies without absorption. The upper and lower 68% uncertainty contours for the *Fermi* data are shown as red dashed and blue dash-dotted lines, respectively. Each of them were also extended with the level of EBL that best fitted the VHE data, which corresponded to a redshift of $z = 0.79$ for the upper contour and to a redshift of $z = 0.70$ for the lower contour. Their unabsorbed extensions to higher energies are shown as red and blue dotted lines.

(A color version of this figure is available in the online journal.)

(2007) resulting in an upper limit of $z < 0.78$. Mazin & Goebel (2007) combined all of the existing VHE gamma-ray data from PG 1553+113 and, by assuming that a break in the intrinsic spectrum should be visible if the source lies above $z = 0.42$, as well as a limit on the hardness of the intrinsic spectrum $\Gamma_{\rm int} = 1.5$, placed an upper limit of $z < 0.42$ on the redshift of PG 1553+113.

The gamma-ray SED measured by *Fermi*, H.E.S.S., and MAGIC are plotted together in Figure 3. The VHE data are non-simultaneous with those from *Fermi* and comprise two H.E.S.S. data sets and two MAGIC data sets (Aharonian et al. 2006b, 2008; Albert et al. 2007, 2009). The VHE spectra recorded by H.E.S.S. and by MAGIC were consistent during all observations. Although one of the MAGIC data sets showed evidence for a change in the mean flux level from PG 1553+113 on month timescales, no evidence for strong variability or day-scale (or shorter) VHE flux variability is seen, within the measurement uncertainties, in any of the data sets. As described in Section 2, no flux or spectral variability was detected in the *Fermi* data set. We therefore make the assumption here that the source was in a non-flaring state during all of the gamma-ray observations. Furthermore, since the highest energy *Fermi* data points, which overlap with the energy range covered by MAGIC, show a flux level consistent with that measured by MAGIC, we assume that PG 1553+113 was in a similar flux and spectral state at all epochs plotted in Figure 3. We note that in both the optical and X-ray regimes, the spectral properties of PG 1553+113 were not seen to change significantly even when its flux level changed.

The spectrum measured by *Fermi* is best fit by a simple power law. We make the assumption that any departures from this power-law spectrum up to 1 TeV are dominated by absorption of gamma rays by the EBL and use the parameterization of Franceschini et al. (2008), which includes evolutionary effects, to find the level of EBL, and therefore the redshift, which best fits the measured data. By absorbing the extrapolated *Fermi* spectrum with EBL corresponding to redshifts from $z = 0.01$ to 3.00, in steps of $z = 0.01$, we find that a redshift of $z = 0.75$ gives the best χ^2 fit to the measured VHE data for the EBL model of Franceschini et al. (2008). When the *Fermi* 68% uncertainty contours, derived from Equation 3, are subjected to the same fitting procedure as the power-law spectrum, we obtain the statistical error on the redshift determination for the Franceschini et al. (2008) EBL giving us a range from $z = 0.70$ to 0.79, as illustrated in Figure 3. Since the model of Franceschini et al. (2008) provides the lowest level for the EBL over the range of interest here, the redshift derived from it should be considered an upper limit. Due to the fact that we performed this calculation for just one parameterization of the EBL, we do not estimate the systematic uncertainty associated with absorbing the *Fermi* spectrum with different EBL models and we discuss this further in Section 5. We note that the systematic uncertainty on the energy scale, which is on the order of 10%–15% for the VHE gamma-ray telescopes (Aharonian et al. 2006c; Albert et al. 2008), was not taken into account in these calculations.

4. DISCUSSION

The *Fermi* data presented here allowed us to derive the longest, continuously sampled light curves to date for

PG 1553+113. Its flux in this energy regime is such that its variability can be probed on ∼day timescales. The combination of the low duty cycle of VHE instruments and the weak flux from PG 1553+113 at those energies means that the timescales accessible with the LAT for this source are shorter than those accessible at higher energies where longer integration times than those available on nightly timescales have been necessary to achieve a significant detection. No evidence for variability was found in the *Fermi* integral flux and photon index light curves. That there is no evidence for variability from PG 1553+113 is consistent with observations of other BL Lacs with *Fermi* and the VHE instruments. The recently released *Fermi* LBAS (Abdo et al. 2009a) found evidence that BL Lacs are less variable than the other blazar subclass, the flat spectrum radio quasars (FSRQs). Using a simple χ^2 test, 70% of the LBAS FSRQs were found to be variable compared to 29% of the LBAS BL Lacs. Also, the fact that approximately 70% of the EGRET-detected blazars are not in the LBAS, with comparable flux thresholds, is a further indication that high activity in the gamma-ray range is not frequent for a given source. As the number of BL Lacs detected in the VHE regime increases, it seems that these objects are not all as variable in the VHE regime as initial observations of Markarian 421 and Markarian 501 suggested (e.g., Buckley et al. 1996, Gaidos et al. 1996, Aharonian et al. 1997, Quinn et al. 1999). Of the 21 BL Lacs now confirmed to be VHE gamma-ray emitters[60] (Wakely & Horan 2008), 10 (48%) have, to date, shown no evidence for strong variability, 4 (19%) have shown marginal evidence for variability (i.e., different flux levels on yearly timescales), and 7 (33%) show strong evidence for variability. It should be noted, however, that selection effects can play a role here: the low duty cycles and small fields of views of VHE instruments limits their ability to perform routine monitoring of a large sample of sources and, in many cases, BL Lac observations are triggered by high flux states. *Fermi*, on the other hand, with its large field of view and high duty cycle, can sample the light curves of sources in a more even fashion, in particular over day-scale timebins. It is, however, less sensitive than VHE instruments to shorter term variability of sources with spectral and flux characteristics typical of BL Lacs detected to date. Threshold effects, also, can play a role in the detection of variability from a source. When the falling edge of the source's SED intersects with the low energy range of the instrument sensitivity (this is the case for the FSRQs with *Fermi* and the BL Lacs with the VHE instruments), a slight spectral shift from the source can mimic the effects of a large level of variability.

4.1. Modeling the Intrinsic Emission of PG 1553+113

In accordance with the weak observed variability, all of the available PG 1553+113 gamma-ray data were combined in turn with each of the X-ray data sets and, assuming a redshift of $z = 0.75$ as found above, each data set was modeled with a single-zone synchrotron self-Compton (SSC) model, that is, a scenario in which one population of electrons is responsible for the broadband emission, producing synchrotron radiation in the radio to X-ray regime and upscattering these synchrotron photons to produce the gamma-ray emission (Band & Grindlay 1985; the model employed here is similar to the one used in Aharonian et al. 2009). Figure 4 shows the result of this fitting. The electrons are parameterized as a three-component power law, $dn/d\gamma \propto \gamma^{-p_i}$ ($i = 1$–3), with minimal and maximal Lorentz factors $\gamma_{\rm min}$ and $\gamma_{\rm max}$, break Lorentz factors of γ_1 and γ_2, and total electron number of $D_{\rm tot}$. For each of the X-ray data sets, the SED was modeled by finding the parameters of the electron distribution that provided a good fit to the shape of the low-energy component (radio to X-ray), while keeping the same values for the emitting region radius, R, the magnetic field strength, B, and the bulk Doppler factor, $\delta_{\rm bulk}$ throughout. This fitting procedure resulted in values of $R = 1.4 \times 10^{18}$ cm, $B = 0.01$ Gauss, and $\delta_{\rm bulk} = 32$. Table 3 lists the best-fit values of the electron parameters for each of the X-ray data sets. A zoom of the high-energy component of the SED for the *Fermi* data with the data set that is most simultaneous (that corresponding to the KVA, *Suzaku*, and VHE data from 2006 July), without the effects of EBL absorption, is shown in Figure 5. It can be seen that, even with the presence of the intrinsic curvature that is inherent to the SSC model, most of the curvature in the high-energy portion of the spectrum can be accounted for by EBL absorption.

Table 3
The Parameters of the Electron Distribution in the SSC Model, as Described in the Text, Used to Fit the PG 1553+113 Data

Model Parameter	*RXTE* (Blue)	*Swift-XRT* (Yellow)	*Suzaku* (Green)	*Swift-XRT* (Magenta)	No X-rays (Black)
	2003 Apr/May	2005 Oct	2006 Jul	2009 Mar	...
p_1	1.70	1.70	1.70	1.70	1.70
p_2	3.00	3.00	2.70	3.00	3.00
p_3	4.10	4.10	3.90	4.10	...
$\gamma_{\rm max} \times 10^6$	3.16	3.16	3.16	3.16	0.20
$\gamma_1 \times 10^4$	6.59	6.59	6.59	5.07	5.71
$\gamma_2 \times 10^4$	7.61	22.8	7.61	6.59	...
$D_{\rm tot} \times 10^{54}$	4.00	3.70	3.93	4.28	4.32

Notes. The dates of the observations are listed at the top of each column. The color of the line used to show each of the models in Figure 4 is listed in parenthesis beneath each column's header. For each data set, the minimal Lorentz factor is $\gamma_{\rm min} = 1.00$ and we find an equipartition factor of 0.2 (ratio of the energy density in the magnetic field to that in the particles of the jet).

We found that this simple, one-zone SSC model provided a reasonably good fit to the PG 1553+113 SED. By altering only the distribution of the electrons that produce the synchrotron emission, a good fit to the overall SED was found for each of the X-ray flux states; and for all of these model realizations, the VHE component of the SED did not change significantly: the magnitude of the changes in the SED above ∼200 GeV are on the order of the VHE statistical measurement uncertainties. This consistency of spectral shape implies that the gamma-ray flux could remain consistent with the state seen by H.E.S.S. and MAGIC during the observations of 2005–2006, even in the presence of the large changes in the X-ray flux level that have been detected. Such behavior was also observed with simultaneous data sets from PKS 2155-304 by Aharonian et al. (2009). In a quiescent state during these observations, no correlation was found between its X-ray and VHE gamma-ray fluxes. During previous observations, however, when it was in a flaring state in the gamma-ray regime, there was strong correlation between the X-ray and VHE fluxes (Costamante 2008). This behavior is an indication that the hard X-ray flux of BL Lacs can change significantly without resulting in detectable activity in the gamma-ray regime, except for at the peak of the SED at these energies, i.e., that X-ray variability can be accompanied by VHE gamma-ray quiescence and a measurable

[60] http://tevcat.uchicago.edu; the "Default Catalog," which contains only those sources that have been confirmed as VHE emitters, was used (see TeVCat Web site for more details).

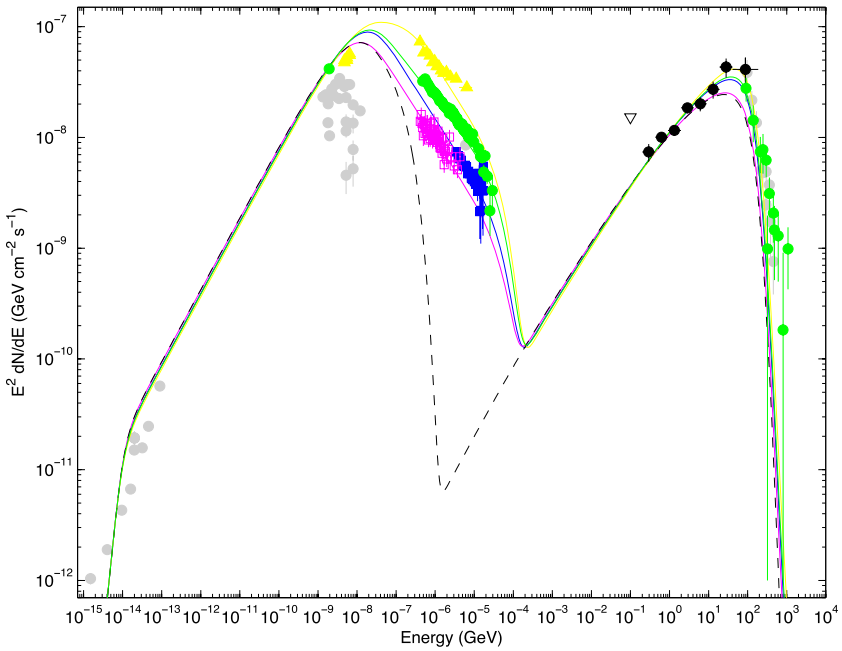

Figure 4. SED for PG 1553+113 fit with an SSC model. The fitting procedure is described in the text. The yellow, green, blue, and magenta lines are, respectively, the SSC model tuned to fit the *Swift-XRT* data, the *Suzaku* data, the *RXTE* data, and the *Swift-XRT* data. The black dashed line is the SSC model when the highest energy electrons are omitted entirely from the fit. The parameters are described in the text and are summarized along with the dates of the observations in Table 3. The X-ray data have been de-absorbed for a column density of $N_H = 3.67 \times 10^{-20}$ cm^{-2}. Apart from 7 hr of the H.E.S.S. data (taken in 2006 April), the KVA (optical; Reimer et al. 2008), *Suzaku* (Reimer et al. 2008), MAGIC (Albert et al. 2009), and H.E.S.S. (Aharonian et al. 2008) observations were made in 2006 July and are thus quasi-simultaneous. They are shown as green filled circles. The *Swift-XRT* and *UVOT* data from 2005 October (Tramacere et al. 2007) are shown as yellow triangles while the magenta open squares are *Swift-XRT* data (*Swift* observation ID 31368001) from 2009 March. The *RXTE* data from Osterman et al. (2006) are shown as blue filled squares. The archival data (gray filled circles) come from: Bennett et al. (1986), Becker et al. (1991), Gregory & Condon (1991), Douglas et al. (1996), Gorshkov et al. (2003), (*radio*); Falomo & Treves (1990), Urry et al. (2000), Sbarufatti et al. (2006), the Sloan Digital Sky Survey (Abazajian et al. 2009) via NED, Fox et al. (2006), Tramacere et al. (2007), (*optical-UV*); Donato et al. (2005), (*X-ray*); H.E.S.S. (Aharonian et al. 2008) and Albert et al. (2007), (*VHE gamma ray*).

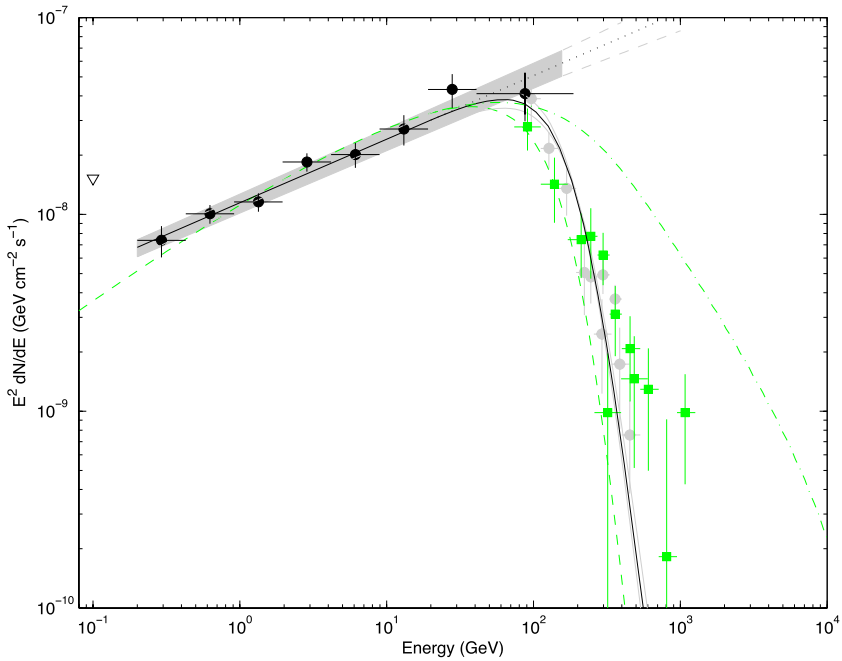

Figure 5. Zoom on the high-energy portion of the SED for PG 1553+113. The *Fermi* data points are shown by black filled circles; the 2006 H.E.S.S. and MAGIC data are shown as green solid squares while the H.E.S.S. and MAGIC data from 2005 are shown as gray solid circles. The EGRET upper limit is shown as a black triangle. The best SSC model fit for the *Suzaku* X-ray data set, with EBL absorption applied, is shown as a green dashed line. The green dash-dotted line shows the SSC model before absorption for the EBL. The black solid line shows the *Fermi* power-law spectrum absorbed for $z = 0.75$ using the model of Franceschini et al. (2008), while the dotted black line shows the unabsorbed *Fermi* spectrum. The shaded area shows the *Fermi* butterfly and the gray dashed lines, its unabsorbed extension to higher energies. The gray solid lines show the *Fermi* butterfly absorbed for the best-fit redshift to each edge, as discussed in Section 3.

shift in the spectrum at the peak of the *Fermi* energy regime. In such a scenario, the electrons producing the variable X-ray emission are at higher energies than those upscattering the bulk of the synchrotron photons to the VHE gamma-ray regime; the scatterings of the variable hardest X-rays are suppressed mostly due to Klein–Nishina effects but also because of the decreasing target photon density at these energies. This effect is demonstrated for the extreme case in Figure 4 where the black dashed curve shows the broadband spectrum when the high-energy electron component is omitted. It can be seen that the difference between it and the curves in which the highest energy electrons are included is still on the order of the statistical measurement uncertainties in the VHE regime.

In the framework of this model, the X-ray and VHE gamma-ray fluxes would be correlated during gamma-ray flaring states while during the more common gamma-ray quiescent states changes in the X-ray flux would not lead to detectable changes in the gamma-ray flux, except for at the high-energy peak in the SED. The simple, one-zone SSC model employed here allows for such a scenario—accounting for the X-ray flux variations observed historically while not requiring detectable changes in the VHE gamma-ray flux state. It provides a good fit to the VHE gamma-ray data with each of the low-energy data sets, only one of which, drawn in green in Figure 4, is quasi-simultaneous (the KVA, *Suzaku*, and all but 7 hr of the VHE data are from 2006 July). It remains to be seen whether such behavior is observed, in general, from BL Lacs, an investigation that can be undertaken jointly by *Fermi* and the X-ray and VHE observatories. Correlations between the arrival of >100 GeV photons in the *Fermi* data and increasing of the hard X-ray flux, in the absence of VHE variability, would be indicative of the proposed scenario. Such effects would be difficult to pin down, however, due to the low rate of detection of >100 GeV photons with *Fermi*.

Vercellone et al. (2004) studied the duty cycle of gamma-ray blazars by comparing the sources detected by EGRET with a sample of radio-selected candidate gamma-ray blazars. They found that most blazars have a duty cycle of less than 10%, meaning that they spend more than 90% of their time in a non-flaring gamma-ray state. The gamma-ray data presented here suggest that PG 1553+113 was in such a state in the *Fermi* energy range during all of these observations. Given the increase in sensitivity and duty cycle afforded us by *Fermi*, we should expect to detect many more blazars in their quiescent states in the >200 MeV energy range.

5. CONCLUSION

We have combined the *Fermi* data from PG 1553+113 with data from radio through VHE gamma rays to study its broadband emission. We demonstrated that a simple, one-zone SSC model provides a reasonably good fit to the observational results: it accounts for the different X-ray flux states observed while also allowing the gamma-ray data to remain approximately constant. More detailed theoretical modeling of the SED, which naturally might fit the data points better, is beyond the scope of this paper.

We have used gamma-ray data spanning 4 orders of magnitude to seek the EBL column density (as parameterized by Franceschini et al. 2008) that best fits the measured spectrum of PG 1553+113. We find that an EBL integrated to a redshift of $z = 0.75^{+0.04}_{-0.05}$ provides the best fit. Such a high value for the redshift would make PG 1553+113 the most distant source to be detected in the VHE regime, an attribute consistent with it being the VHE source with the largest spectral break in the gamma-ray regime ($\Gamma_{\rm VHE} - \Gamma_{\rm HE} \sim 2.7$). Three assumptions were made in our redshift calculation. The first one was that the EBL behaves in a manner consistent with the model of Franceschini et al. (2008). Of the many EBL models available in the literature (see Finke & Razzaque 2009 for a recent comparison), that of Franceschini et al. (2008) predicts the lowest level of EBL across the energy range of interest here; it provides the minimum level of EBL photons that could exist based on known sources alone and therefore, in using it, the redshift derived for PG 1553+113 can be considered an upper limit. Had one of the other EBL models been used, the best-fit redshift would have been lower. Indeed, a more in-depth study of the absorption effects of the EBL on the spectrum of PG 1553+133 should consider all of the EBL models available in the literature. In this way, the systematic effects of using different realizations of the EBL could be determined; the data points provided in Table 2 allow for such a study to be undertaken.

Two additional assumptions were made in our redshift calculation, first, that the emission state of PG 1553+113 did not change significantly during the gamma-ray observations, which can be interpreted as an indication that it was in a low-flux state at these energies throughout those observations. Indeed, the quiescent state is the state in which we are most likely to find a blazar (Vercellone et al. 2004). Second, it was assumed that the power-law spectrum measured by *Fermi* does not suffer from significant intrinsic absorption up to 1 TeV. Should there be intrinsic absorption of VHE gamma rays at the source, a lower level of EBL absorption would be required to best fit the measured VHE spectrum. We note that, since the *Fermi* data show no evidence for spectral curvature, if it is significant intrinsic absorption that is mostly responsible for the sharp break in the gamma-ray spectrum, its effects would have to kick in at energies exactly above those accessible to *Fermi* and, at a significant level, in order to produce the sharp break observed in the data.

This is the first time that the measurement of the complete HE to VHE gamma-ray spectrum of a source has been used to constrain its redshift. The value derived here is close to the limits derived by Aharonian et al. (2008) and Albert et al. (2007) and is higher than that derived by Mazin & Goebel (2007). Different parameterizations of the EBL were used in these analyses (those of Kneiske et al. 2004 and Primack et al. 2001), so this is one of the factors contributing to the different results. Additionally, for these previous redshift constraints using gamma-ray data, it was necessary to make assumptions about the hardness of the intrinsic spectrum in the HE regime. The *Fermi* measurement of the HE spectrum from PG 1553+113 allows us to reduce the number of assumptions used in the constraining the redshift. Combining the *Fermi* measurement with the measured VHE spectra affords us complete coverage of the PG 1553+113 SED from 200 MeV to 1.1 TeV.

Its potentially large distance together with its consistently detectable gamma-ray flux make PG 1553+113 an excellent candidate with which to search for EBL cascading effects first proposed by Protheroe (1986), and subsequently explored by many authors (e.g., Protheroe & Stanev 1993; Aharonian et al. 1994; Biller 1995; D'Avezac et al. 2007; Elyiv et al. 2009). If present, pile-up from such cascades is predicted to occur below 100 GeV. Some authors predict that cascades produce a characteristic spectral bump, which could be detectable in the *Fermi* energy regime if the strength of the extragalactic magnetic field in the direction of the source being studied is

less than $B = 10^{-6}$ nG (D'Avezac et al. 2007). Elyiv et al. (2009) predict that, for magnetic field strengths of $B \leqslant 10^{-7}$ nG, extended emission due to the cascading of the source photons should be detectable around extragalactic gamma-ray sources by *Fermi*.

The possibility that PG 1553+113 could be a particularly distant TeV source provides further impetus for IR/optical/UV astronomers to revisit the redshift measurement. A direct measurement would be very welcome, and would ultimately settle the question of the accuracy of estimates based on the EBL. The *Fermi* LAT is continuing to accumulate data on PG 1553+113. Subsequent studies of these data will, therefore, allow us to measure its spectral shape with greater sensitivity at the highest energies accessible to *Fermi*.

The *Fermi* LAT Collaboration acknowledges the generous support of a number of agencies and institutes that have supported the *Fermi* LAT Collaboration. These include the National Aeronautics and Space Administration and the Department of Energy in the United States; the Commissariat à l'Energie Atomique and the Centre National de la Recherche Scientifique/Institut National de Physique Nucléaire et de Physique des Particules in France; the Agenzia Spaziale Italiana and the Istituto Nazionale di Fisica Nucleare in Italy; the Ministry of Education, Culture, Sports, Science and Technology (MEXT), High Energy Accelerator Research Organization (KEK), and Japan Aerospace Exploration Agency (JAXA) in Japan; and the K. A. Wallenberg Foundation, the Swedish Research Council, and the Swedish National Space Board in Sweden. Additional support for science analysis during the operations phase from the following agencies is also gratefully acknowledged: the Istituto Nazionale di Astrofisica in Italy and the K. A. Wallenberg Foundation in Sweden. This research has made use of the NASA/IPAC Extragalactic Database (NED) which is operated by the Jet Propulsion Laboratory, California Institute of Technology, under contract with the National Aeronautics and Space Administration. This research has made use of the SIMBAD database, operated at CDS, Strasbourg, France. Thanks to Wystan Benbow, Luigi Costamante, Daniela Dorner, Andrea Tramacere, and Robert Wagner for supplying archival data points.

Facilities: Fermi (LAT)

REFERENCES

Abazajian, K. N., et al. 2009, ApJS, 182, 543
Abdo, A. A., et al. 2009a, ApJ, 700, 597
Abdo, A. A., et al. 2009b, ApJS, 183, 46
Aharonian, F., et al. 1997, A&A, 327, L5
Aharonian, F., et al. 2006a, Nature, 440, 1018
Aharonian, F., et al. 2006b, A&A, 448, L19
Aharonian, F., et al. 2006c, A&A, 457, 899
Aharonian, F., et al. 2008, A&A, 477, 481
Aharonian, F., et al. 2009, ApJ, 696, L150
Aharonian, F. A., Coppi, P. S., & Voelk, H. J. 1994, ApJ, 423, L5
Albert, J., et al. 2007, ApJ, 654, L119
Albert, J., et al. 2008, ApJ, 674, 1037
Albert, J., et al. 2009, A&A, 493, 467
Atwood, W. B., et al. 2009, ApJ, 697, 1071
Band, D. L., & Grindlay, J. E. 1985, ApJ, 298, 128
Becker, R. H., White, R. L., & Edwards, A. L. 1991, ApJS, 75, 1
Beckmann, V., Wolter, A., Celotti, A., Costamante, L., Ghisellini, G., Maccacaro, T., & Tagliaferri, G. 2002, A&A, 383, 410
Bennett, C. L., Lawrence, C. R., Burke, B. F., Hewitt, J. N., & Mahoney, J. 1986, ApJS, 61, 1
Biller, S. D. 1995, Astropart. Phys., 3, 385
Buckley, J. H., et al. 1996, ApJ, 472, L9
Carangelo, N., Falomo, R., Kotilainen, J., Treves, A., & Ulrich, M.-H. 2003, in ASP Conf. Ser. 299, High Energy Blazar Astronomy, ed. L. O. Takalo & E. Valtaoja (San Francisco, CA: ASP), 299
Costamante, L. 2008, Int. J. Mod. Phys. D, 17, 1449
Costamante, L., Aharonian, F., Horns, D., & Ghisellini, G. 2004, New Astron. Rev., 48, 469
D'Avezac, P., Dubus, G., & Giebels, B. 2007, A&A, 469, 857
Donato, D., Ghisellini, G., Tagliaferri, G., & Fossati, G. 2001, A&A, 375, 739
Donato, D., Sambruna, R. M., & Gliozzi, M. 2005, A&A, 433, 1163
Douglas, J. N., Bash, F. N., Bozyan, F. A., Torrence, G. W., & Wolfe, C. 1996, AJ, 111, 1945
Dwek, E., & Krennrich, F. 2005, ApJ, 618, 657
Elyiv, A., Neronov, A., & Semikoz, D. 2009, Phys. Rev. D, 80, 023010
Falomo, R., Scarpa, R., & Bersanelli, M. 1994, ApJS, 93, 125
Falomo, R., & Treves, A. 1990, PASP, 102, 1120
Finke, J. D., & Razzaque, S. 2009, ApJ, 698, 1761
Fox, A. J., Savage, B. D., & Wakker, B. P. 2006, ApJS, 165, 229
Franceschini, A., Rodighiero, G., & Vaccari, M. 2008, A&A, 487, 837
Gaidos, J. A., et al. 1996, Nature, 383, 319
Gorshkov, A. G., Konnikova, V. K., & Mingaliev, M. G. 2003, Astron. Rep., 47, 903
Green, R. F., Schmidt, M., & Liebert, J. 1986, ApJS, 61, 305
Gregory, P. C., & Condon, J. J. 1991, ApJS, 75, 1011
Hartman, R. C., et al. 1999, ApJS, 123, 79
Hutchings, J. B., & Neff, S. G. 1992, AJ, 104, 1
Kneiske, T. M., Bretz, T., Mannheim, K., & Hartmann, D. H. 2004, A&A, 413, 807
Krennrich, F., Dwek, E., & Imran, A. 2008, ApJ, 689, L93
Massaro, F., Tramacere, A., Cavaliere, A., Perri, M., & Giommi, P. 2008, A&A, 478, 395
Mazin, D., & Goebel, F. 2007, ApJ, 655, L13
Miller, H. R., & Green, R. F. 1983, BAAS, 15, 957
O'Dowd, M., & Urry, C. M. 2005, ApJ, 627, 97
Osterman, M. A., et al. 2006, AJ, 132, 873
Perlman, E. S., et al. 2005, ApJ, 625, 727
Primack, J. R., Somerville, R. S., Bullock, J. S., & Devriendt, J. E. G. 2001, in AIP Conf. Ser. 558, High Energy Gamma-ray Astronomy, ed. F. A. Aharonian (Melville, NY: AIP), 463
Protheroe, R. J. 1986, MNRAS, 221, 769
Protheroe, R. J., & Stanev, T. 1993, MNRAS, 264, 191
Quinn, J., et al. 1999, ApJ, 518, 693
Rector, T. A., Gabuzda, D. C., & Stocke, J. T. 2003, AJ, 125, 1060
Reimer, A., Costamante, L., Madejski, G., Reimer, O., & Dorner, D. 2008, ApJ, 682, 775
Sbarufatti, B., Treves, A., & Falomo, R. 2005, ApJ, 635, 173
Sbarufatti, B., Treves, A., Falomo, R., Heidt, J., Kotilainen, J., & Scarpa, R. 2006, AJ, 132, 1
Scarpa, R., Urry, C. M., Falomo, R., Pesce, J. E., & Treves, A. 2000, ApJ, 532, 740
Stecker, F. W., Baring, M. G., & Summerlin, E. J. 2007, ApJ, 667, L29
Strong, A. W., Moskalenko, I. V., & Reimer, O. 2004a, ApJ, 613, 962
Strong, A. W., Moskalenko, I. V., Reimer, O., Digel, S., & Diehl, R. 2004b, A&A, 422, L47
Tramacere, A., et al. 2007, A&A, 467, 501
Treves, A., Falomo, R., & Uslenghi, M. 2007, A&A, 473, L17
Urry, C. M., Scarpa, R., O'Dowd, M., Falomo, R., Pesce, J. E., & Treves, A. 2000, ApJ, 532, 816
Vaughan, S., Edelson, R., Warwick, R. S., & Uttley, P. 2003, MNRAS, 345, 1271
Vercellone, S., Soldi, S., Chen, A. W., & Tavani, M. 2004, MNRAS, 353, 890
Wakely, S. P., & Horan, D. 2008, in Proc. of 30th International Cosmic Ray Conf., Vol. 3, ed. R. Caballero, et al. (Mexico City: Universidad Nacional Autónoma de México), 1341